Predicting Reconstruction Quality Within Compressive Sensing for Atomic Force Microscopy

Patrick Steffen Pedersen, Jan Østergaard, and Torben Larsen
Department of Electronic Systems, Faculty of Engineering and Science, Aalborg University
DK-9220 Aalborg, Denmark

***Abstract*—With compressive sensing, the obtainable reconstruction quality depends on the original signal, the reconstruction algorithm, the measurement matrix, and the dictionary matrix. The present paper is concerned with establishing performance indicators and using these to predict reconstruction quality in atomic force microscopy applications. For this purpose, we consider the well-known quantities of coherence and mutual coherence. Furthermore, we propose a new performance indicator derived from coherence in order to better model the average reconstruction quality. Through extensive simulations, affine models using the performance indicators are evaluated in terms of modified coefficients of determination. The results show that the proposed performance indicator yields a better model than both coherence and mutual coherence do. In conclusion, the proposed performance indicator can be used to predict reconstruction quality for the given application, and the affine prediction model can be improved by including coherence and mutual coherence.**

I. Introduction

Atomic force microscopy (AFM) is an advanced tool for investigating and manipulating the surface of nanoscale matter [1], [2], [3], [4]. In particular, AFM is used for high-resolution imaging resulting in 3D surface maps with, potentially, sub-nanometer resolution [5]. In order to do so, a sharp probe is brought close to the surface, and the probe and surface are moved relative to each other while the force on the surface affects the probe which, loosely speaking, "feels" the surface [6]. Unfortunately, image acquisition takes on the order of minutes to hours using standard AFM imaging [7].

To reduce the data acquisition time of AFM, one approach is to reduce the number of samples using compressive sensing (CS) [8]. This recent signal acquisition paradigm enables certain signals to be accurately reconstructed from fewer samples than dictated by the Nyquist rate [9], [10]. This acquisition does, however, entail solving a non-convex optimisation problem which, in the noiseless case, takes the form [11]:

$$\begin{aligned} &\text{minimise} && ||\hat{\boldsymbol{\alpha}}||_0 \\ &\text{subject to} && \mathbf{y} = \boldsymbol{\Phi}\boldsymbol{\Psi}\hat{\boldsymbol{\alpha}} \end{aligned} \tag{1}$$

where $\mathbf{y} \in \mathbb{R}^{m\times 1}$ is the sampled vector, $\boldsymbol{\Phi} \in \mathbb{R}^{m\times p}$ is a so-called measurement matrix, $\boldsymbol{\Psi} \in \mathbb{C}^{p\times n}$ is a so-called dictionary matrix, and $\hat{\boldsymbol{\alpha}} \in \mathbb{C}^{n\times 1}$ is the reconstructed coefficent vector. That is, $\boldsymbol{\alpha}$ is the signal using $\boldsymbol{\Psi}$ as a base, and the reconstructed signal is thus $\boldsymbol{\Psi}\hat{\boldsymbol{\alpha}} = \hat{\mathbf{x}} \in \mathbb{R}^{p\times 1}$. In the context of AFM, $\mathbf{x}$ contains the pixel values of the image, and $\mathbf{y}$ contains the sampled pixel values.

In order to acquire an image with AFM using CS, the user must choose $\boldsymbol{\Phi}$ and $\boldsymbol{\Psi}$ in (1) as well as an algorithm capable of solving the reconstruction problem. It would be advantageous to know in advance which choices result in consistently high-quality reconstructions across images. This prompts for an image-independent method for predicting the obtainable reconstrution quality. Furthermore, since different use cases benefit from different reconstruction algorithms, the prediction should be independent of the algorithm used. Consequently, the present paper is concerned with predicting reconstruction quality from properties of the measurement matrix and the dictionary matrix, and we refer to these properties as performance indicators.

The literature states two fundamental premises of CS: sparsity and incoherence [12]. The premise of sparsity requires a signal to have a concise representation in a convenient basis. For example, a frequency sparse signal is sparse in the Fourier basis. The premise of incoherence, on the other hand, requires a low maximum correlation between the columns of $\boldsymbol{\Psi}$, known as atoms, and the rows of $\boldsymbol{\Phi}$. For example, the identity matrix is incoherent with the Fourier basis. In terms of mutual coherence, $\mu_{\text{mut}}(\boldsymbol{\Phi}, \boldsymbol{\Psi})$, the premise states that, generally [12]:

$$\mu_{\text{mut}}(\boldsymbol{\Phi}, \boldsymbol{\Psi}) \ll 1 \tag{2}$$

for normalised $\boldsymbol{\Phi}$ and $\boldsymbol{\Psi}$ where $\mu_{\text{mut}}(\boldsymbol{\Phi}, \boldsymbol{\Psi})$ is defined as:

$$\mu_{\text{mut}}(\boldsymbol{\Phi}, \boldsymbol{\Psi}) = \max_{1\leq i\leq m, 1\leq j\leq n} |\boldsymbol{\Phi}_{i,:}\boldsymbol{\Psi}_{:,j}| \tag{3}$$

Partly due to CS being a mathematically well-defined paradigm, theoretical guarantees exist which could conceivably be used for predicting reconstruction quality. Most of these guarantees relate to the restricted isometry property (RIP) [13], which cannot be computed without solving yet another non-convex optimisation problem in the general case [13]. Alternatively, bounds on RIP can be established which

rely on, for example, the coherence, $\mu_{\text{coh}}(\mathbf{A})$ with $\mathbf{A} = \mathbf{\Phi\Psi}$ [13]:

$$\mu_{\text{coh}}(\mathbf{A}) = \max_{1 \leq i \neq j \leq n} \frac{|\mathbf{A}_{:,i}^T \mathbf{A}_{:,j}|}{||\mathbf{A}_{:,i}||_2 ||\mathbf{A}_{:,j}||_2} \tag{4}$$

However, a theoretical guarantee is concerned with worst-case reconstruction problems, whereas the predictions of interest should represent the average reconstruction problems. As expected, the theoretical guarantees result in unnecessarily pessimistic predictions for such problems [14].

For a more accurate prediction model, performance indicators are of interest. As the quantity behind a premise of CS which depends only on $\mathbf{\Phi}$ and $\mathbf{\Psi}$, $\mu_{\text{mut}}(\mathbf{\Phi}, \mathbf{\Psi})$ is considered a performance indicator candidate. Another candidate is $\mu_{\text{coh}}(\mathbf{A})$. Finally, we propose a third candidate, the coherence 2-norm, inspired by coherence but using an alternative norm.

Based on the performance indicators of mutual coherence, coherence, and coherence 2-norm, we have attempted to establish a simple affine model to predict the reconstruction quality within CS for AFM. A large number of simulations were performed to estimate the parameters of the model and evaluate both the model and the performance indicators. The simulations include a number of images, reconstruction algorithms, measurement matrices, and dictionary matrices. The results show that, in terms of modified R^2, the proposed performance indicator yields a better model than the other performance indicators do. Furthermore, the model is improved when all three performance indicators are used in combination.

The paper is organised as follows: In Section II, we revisit coherence and mutual coherence as performance indicators in the current context and define coherence 2-norm. Section III describes the setup used for simulations whereas Section IV presents the simulation results. We discuss these results in Section V and finally draw conclusions and discuss future work in Section VI.

II. Indicators

With the given application, certain constraints are put on $\mathbf{\Phi}$ because of the physical limitations of AFM. Since the probe tip only measures a single point at a time, each measurement pertains to a single pixel making the measurement matrix extremely sparse. That is, each row of $\mathbf{\Phi}$ is a zero vector except from a single entry containing the value, one. Furthermore, we assume that the same pixel is not included more than once in $\mathbf{y}$. That is, each column of $\mathbf{\Phi}$ contains at most one non-zero entry.

As mentioned in Section I, the mutual coherence describes the maximum correlation between the columns of $\mathbf{\Psi}$ and the rows of $\mathbf{\Phi}$. With the constraints on $\mathbf{\Phi}$, the mutual coherence is simply the maximum absolute value of the entries in $\mathbf{\Psi}$ on the subset of rows dictated by $\mathbf{\Phi}$. For consistency with the other performance indicators, the definition is slightly rewritten:

$$\mu_{\text{mut}}(\mathbf{\Phi}, \mathbf{\Psi}) = \max_{1 \leq i \leq m, 1 \leq j \leq n} |\mathbf{\Phi}_{i,:} \mathbf{\Psi}_{:,j}| \tag{5}$$

The coherence describes the maximum correlation between two columns of $\mathbf{A} = \mathbf{\Phi\Psi}$. With the constraints on $\mathbf{\Phi}$, the coherence is simply the maximum correlation between two columns of $\mathbf{\Psi}$ with only the entries dictated by $\mathbf{\Phi}$. For consistency with the other performance indicators, the definition is slightly rewritten:

$$\mu_{\text{coh}}(\mathbf{\Phi}, \mathbf{\Psi}) = \max_{1 \leq i \neq j \leq n} \frac{|\mathbf{\Psi}_{:,i}^T \mathbf{\Phi}^T \mathbf{\Phi\Psi}_{:,j}|}{||\mathbf{\Phi\Psi}_{:,i}||_2 ||\mathbf{\Phi\Psi}_{:,j}||_2} \tag{6}$$

However, the infinity-norm used in (4) is introduced to ensure a theoretical bound on RIP. In practise, other coherence values might influence the reconstruction quality than merely the maximum coherence value. Motivated by this, we introduce the coherence 2-norm, μ_{rms}:

$$\mu_{\text{rms}}(\mathbf{\Phi}, \mathbf{\Psi}) = \sqrt{\frac{1}{n^2 - n} \sum_{i=1}^{n} \sum_{\substack{j=1 \\ j \neq i}}^{n} \left(\frac{|\mathbf{\Psi}_{:,i}^T \mathbf{\Phi}^T \mathbf{\Phi\Psi}_{:,j}|}{||\mathbf{\Phi\Psi}_{:,i}||_2 ||\mathbf{\Phi\Psi}_{:,j}||_2} \right)^2} \tag{7}$$

III. Simulations

In order to predict reconstruction quality, a model must be established, and the parameters of this model must be estimated. Therefore, we have conducted an extensive set of experiments consisting of all combinations across a set of images, `X`, a set of sampling patterns, `PHI`, a set of dictionaries, `PSI`, and a set of reconstruction algorithms, `R`. For each experiment, the reconstruction problem is solved, the reconstruction quality is computed, and the values of the set of performance indicators, `C`, are calculated.

The image material is based on seven images of biological cells. These images have been acquired with a resolution of 512×512 pixels on Keysight Technologies ILM6000 and ILM7500 AFM equipment. Using a square matrix for dictionary matrix, this resolution results in $\mathbf{\Psi} \in \mathbb{C}^{512^2 \times 512^2}$ which takes up $1\,\text{TiB}$ of memory, when represented with $64\,\text{bit}$ floats. To make the involved computations feasible, the images have been subsequently down-sampled to 128×128 pixels. In addition to these, the set of images, `X`, consists of all non-overlapping 64×64 pixel blocks and all non-overlapping 32×32 pixel blocks of the down-sampled images. Thus, the resulting `X` contains 147 images.

The sampling patterns are based on raster-shaped, square-spiral-shaped [2], spiral-shaped [4], and Lissajous-shaped scanning paths [3]. The set of sampling patterns, `PHI`, consists of matrix representations of these scanning paths using varying undersampling ratios:

$$\delta \in \{0.1 + i \cdot 0.025 | i = 0, \ldots, 8\} \tag{8}$$

The set of dictionaries, `PSI`, consists of the discrete cosine transform (DCT) and the discrete Fourier transform (DFT). The set of reconstruction algorithms, `R`, consists of the iterative hard thresholding (IHT) algorithm [15], the iterative soft thresholding (IST) algorithm [16], and an ℓ_1-minimisation algorithm [17]. Finally, the set of performance

indicators, $\mathtt{C}$, consists of the performance indicators presented in Section II.

Before performing the actual reconstruction, the given image is sampled using the measurement matrix. The sampled image is then detilted by least-squares-fitting and subtracting a plane. This plane is also subtracted from the original image before computing the reconstruction quality. For the actual implementation, the Magni software package [18] is used to read the AFM data files, generate the sampling patterns, generate the measurement and dictionary matrices, perform most of the image reconstructions, evaluate the reconstruction quality, and visualise the results. For the ℓ_1-minimisation image reconstructions, Douglas-Rachford splitting is used as implemented in the PyUNLocBox package[1]. The metric used to asses the reconstruction quality is the peak signal-to-noise-ratio (PSNR) where the peak value, P is the maximum possible pixel value:

$$\text{PSNR} = 10 \log_{10} \left(\frac{P^2}{||\mathbf{x} - \hat{\mathbf{x}}||_2^2} \right) \tag{9}$$

Based on the results, as presented in Section IV, we have chosen to model the reconstruction quality affinely in terms of the performance indicators. That is,

$$\hat{q}_i = \sum_k (a_k c_{k,i}) + b \tag{10}$$

where $\hat{q}_i$ is the predicted reconstruction quality for the i^{th} combination of measurement matrix and dictionary matrix, a_k is the coefficient of the k^{th} performance indicator, $c_{k,i}$ is the value of the k^{th} performance indicator for the i^{th} combination of measurement matrix and dictionary matrix, and b is an offset.

The coefficients are estimated using a least-squares-fit, and, in order to evaluate the usefulness of the established model, the coefficient of determination, R^2, is used:

$$R^2 = 1 - \frac{\text{SS}_\text{e}}{\text{SS}_\text{qq}} \tag{11}$$

where SS_{qq} is the total sum of squares, and SS_e is the sum of squares of residuals:

$$\text{SS}_\text{qq} = \sum_{i=1}^{s} \sum_{j=1}^{t_i} (q_{ij} - \bar{q})^2 \tag{12}$$

$$\text{SS}_\text{e} = \sum_{i=1}^{s} \sum_{j=1}^{t_i} (q_{ij} - \hat{q}_i)^2 \tag{13}$$

$$\bar{q} = \frac{1}{\sum_{i=1}^{s} t_i} \sum_{i=1}^{s} \sum_{j=1}^{t_i} q_{ij} \tag{14}$$

where q_{ij} is the reconstruction quality for the i^{th} combination of measurement matrix and dictionary matrix for the j^{th} combination of image and reconstruction algorithm, s is the number of combinations of measurement matrices and dictionary matrices, and t_i is the number of combinations of images and reconstruction algorithms for the i^{th} combination of measurement matrix and dictionary matrix.

There are t_i different PSNR values for the predicted reconstruction quality, $\hat{q}_i$. Obviously, this causes a lower coefficient of determination. This problem is approached by the lack-of-fit sum of squares which divides the sum of squares of residuals into pure error, SS_pe, and lack-of-fit, SS_lof:

$$\text{SS}_\text{e} = \text{SS}_\text{pe} + \text{SS}_\text{lof} \tag{15}$$

$$\text{SS}_\text{pe} = \sum_{i=1}^{s} \sum_{j=1}^{t_i} (q_{ij} - \bar{q}_i)^2 \tag{16}$$

$$\text{SS}_\text{lof} = \sum_{i=1}^{s} t_i (\bar{q}_i - \hat{q}_i)^2 \tag{17}$$

$$\bar{q}_i = \frac{1}{t_i} \sum_{j=1}^{t_i} q_{ij} \tag{18}$$

Inspired by this distinction, we define a modified R^2 measure which compensates for the pure error that is due to having many reconstruction quality values for the same performance indicator values. We use this measure for evaluating the established model:

$$\tilde{R}^2 = 1 - \frac{\tilde{\text{SS}}_\text{lof}}{\tilde{\text{SS}}_\text{qq}} \tag{19}$$

$$\tilde{\text{SS}}_\text{lof} = \sum_{i=1}^{s} (\bar{q}_i - \hat{q}_i)^2 \tag{20}$$

$$\tilde{\text{SS}}_\text{qq} = \sum_{i=1}^{s} (\bar{q}_i - \bar{q})^2 \tag{21}$$

IV. Results

The simulated set of data is visualised in three subplots in Figure 1: each subplot shows the obtained reconstruction qualities, q_{ij}, the average reconstruction qualities, $\bar{q}_i$, and the affine model which predicts the reconstruction qualities, $\hat{q}_i$, plotted against the individual performance indicator values.

Using the set of data, five models of the form given by (10) were analysed: three models using only the mutual coherence, the coherence, and the coherence 2-norm, respectively, one model using the coherence and the coherence 2-norm, and one model using all three performance indicators. For each model, the model parameters were found with a least-squares-fit. Table I lists the resulting parameters along with the $\tilde{R}^2$ value for each model.

V. Discussion

An affine model was chosen for identifying simple relationships between the proposed performance indicators and the reconstruction quality. With a maximum modified coefficient of determination of 0.701 using only three terms, the affine model is deemed reasonable.

[1] Available at https://github.com/epfl-lts2/pyunlocbox.

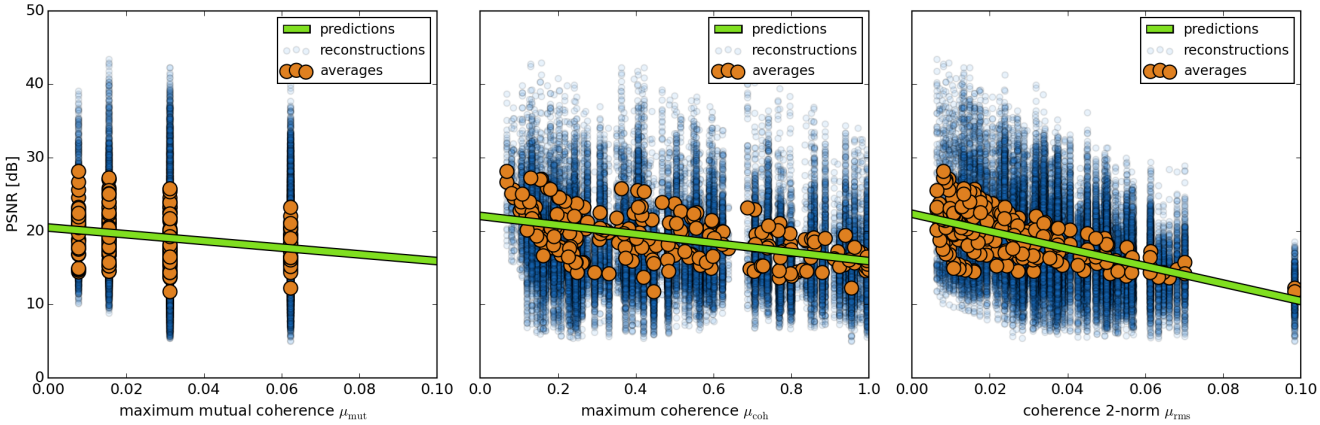

Fig. 1. The obtained PSNR values, q_{ij}, the average obtained PSNR values, $\bar{q}_i$, and PSNR values predicted by the affine model, $\hat{q}_i$, versus the individual performance indicator values for each of the three performance indicators.

TABLE I. MODEL PARAMETERS AND EVALUATION.

Model	a_1	a_2	a_3	b	$\tilde{R}^2$
mut	-45.7	-	-	20.5	0.063
coh	-	-6.15	-	22.0	0.266
rms	-	-	-119	22.3	0.394
coh and rms	-	-4.67	-102	24.0	0.539
combined	107.2	-6.55	-170	23.8	0.701

As shown in Section IV, five models were analysed. Clearly, the models based on the mutual coherence and the coherence performance indicators, respectively, are unable to account for most of the variation in average reconstruction quality. However, the model based on the coherence 2-norm performance indicator is able to account for roughly $40\,\%$ of the variation in average reconstruction quality. Furthermore, the model based on all three performance indicators outperforms the first three models and accounts for the majority of the variation in average reconstruction quality.

With the poor performance of the model based on the mutual coherence performance indicator, the inclusion of this indicator in the final model might not be expected to contribute to a significantly increased $\tilde{R}^2$. For this reason, the model based on the coherence and the coherence 2-norm performance indicators is included. However, interestingly, the model based on all three performance indicators also outperforms the model based on the coherence and the coherence 2-norm performance indicators by rougly $15\,\%$.

From Table I, the values of the coefficients, a_1, a_2, a_3, and b suggest that reconstructions with PSNR values above 25 dB do not occur, at least according to the first four models. However, as indicated by the $\tilde{R}^2$ values, the models do not account for all of the observed variation in reconstruction quality. Furthermore, as seen from Figure 1, the predictions relate to the average PSNR values obtained across multiple images and reconstruction algorithms. Indeed, PSNR values greater than 40 dB were observed in the simulations.

As briefly mentioned in Section I, guarantees exist which relate to RIP which is bounded by an expression relying on the coherence: simply put, the lower the coherence, the better the bound on RIP, and, ultimately, the the better the guarantees on the reconstruction quality. This agrees well with the the trend of the coherence and the coherence 2-norm. On the other hand, as stated in (3), one of the two fundamental premises of CS requires a low mutual coherence. Although the mutual coherence is indeed low, a correlation between higher reconstruction qualities and smaller mutual coherence values might be expected. This expectation does, however, only poorly agree with the vague trend of the mutual coherence.

VI. CONCLUSIONS AND FUTURE WORK

The purpose of the present paper is to predict reconstruction quality from properties of the measurement matrix and the dictionary matrix, referred to as performance indicators. We have suggested the well-known quantities of mutual coherence and coherence as performance indicators and, furthermore, proposed the coherence 2-norm performance indicator. The results presented show that an affine model based on these performance indicators is able to account for the majority of the observed variation in average reconstruction quality.

In the present paper, the performance indicators have been used for establishing a prediction model of the reconstruction quality obtainable in CS problems within AFM. However, the potential of the performance indicators extend beyond this application. With the observed relations between the coherence 2-norm, coherence, and mutual coherence, on one hand, and reconstruction quality, on the other, performance indicators could be used for optimising measurement matrices and/or dictionary matrices. Indeed, coherence has already been proposed in the context of learning algorithms for CS. Potentially, the proposed coherence 2-norm performance indicator could improve such learning algorithms.

REFERENCES

[1] T. Tuma, J. Lygeros, A. Sebastian, and A. Pantazi, "Optimal scan trajectories for high-speed scanning probe microscopy," in *American Control Conference (ACC)*, Montréal, Canada, Jun. 27 – 29, 2012, pp. 3791–3796.

[2] B. Song, N. Xi, R. Yang, K. W. C. Lai, and C. Qu, "Video Rate Atomic Force Microscopy (AFM) Imaging using Compressive Sensing," in *11th IEEE International Conference on Nanotechnology*, Portland, Oregon, USA, Aug. 15-18, 2011, pp. 1056–1059.

[3] T. Tuma, J. Lygeros, V. Kartik, A. Sebastian, and A. Pantazi, "High-speed multiresolution scanning probe microscopy based on Lissajous scan trajectories," *Nanotechnology*, vol. 23, no. 18, p. 9, Apr. 2012.

[4] I. A. Mahmood, S. O. R. Moheimani, and B. Bhikkaji, "A New Scanning Method for Fast Atomic Force Microscopy," *IEEE Transactions on Nanotechnology*, vol. 10, no. 2, pp. 203–216, Mar. 2011.

[5] D. Y. Abramovitch, S. B. Andersson, L. Y. Pao, and G. Schitter, "A Tutorial on the Mechanisms, Dynamics, and Control of Atomic Force Microscopes," in *American Control Conference*, New York City, USA, Jul. 11-13, 2007, pp. 3488–3502.

[6] B. Bhushan and O. Marti, "Scanning Probe Microscopy – Principle of Operation, Instrumentation, and Probes," in *Springer Handbook of Nanotechnology*, B. Bhushan, Ed. Springer Berlin Heidelberg, 2010, ch. 21, pp. 573–617.

[7] Y. K. Yong, A. Bazaei, S. O. R. Moheimani, and F. Allgöwer, "Design and Control of a Novel Non-Raster Scan Pattern for Fast Scanning Probe Microscopy," in *IEEE/ASME International Conference on Advanced Intelligent Mechatronics (AIM)*, Kachsiung, Taiwan, Jul., 11 – 14, 2012, pp. 456–461.

[8] S. B. Andersson and L. Y. Pao, "Non-Raster Sampling in Atomic Force Microscopy: A Compressed Sensing Approach," in *American Control Conference (ACC)*, Montréal, Canada, Jun. 27-29, 2012, pp. 2485–2490.

[9] R. G. Baraniuk, "Compressive sensing [lecture notes]," *IEEE Signal Processing Magazine*, vol. 24, no. 4, pp. 118–121, Jul. 2007.

[10] J. Romberg, "Imaging via Compressive Sampling," *IEEE Signal Processing Magazine*, vol. 25, no. 2, pp. 14–20, Mar. 2008.

[11] E. J. Candès, J. Romberg, and T. Tao, "Robust Uncertainty Principles: Exact Signal Reconstruction From Highly Incomplete Frequency Information," *IEEE Transactions on Information Theory*, vol. 52, no. 2, pp. 489–509, Feb. 2006.

[12] E. J. Candès and M. B. Wakin, "An Introduction To Compressive Sampling," *IEEE Signal Processing Magazine*, vol. 25, no. 2, pp. 21–30, Mar. 2008.

[13] M. F. Duarte and Y. C. Eldar, "Structured Compressed Sensing: From Theory to Applications," *IEEE Transactions on Signal Processing*, vol. 59, no. 9, pp. 4053–4085, Sep. 2011.

[14] D. L. Donoho and J. Tanner, "Precise Undersampling Theorems," *Proceedings of the IEEE*, vol. 98, no. 6, pp. 913–924, Jun. 2010.

[15] T. Blumensath and M. E. Davies, "Iterative Thresholding for Sparse Approximations," *Journal of Fourier Analysis and Applications*, vol. 14, no. 5-6, pp. 629–654, Sep. 2008.

[16] I. Daubechies, M. Defrise, and C. D. Mol, "An Iterative Thresholding Algorithm for Linear Inverse Problems with a Sparsity Constraint," *Communications on Pure and Applied Mathematics*, vol. 57, no. 11, pp. 1413–1457, Nov. 2004.

[17] D. L. Donoho, "Compressed Sensing," *IEEE Transactions on Information Theory*, vol. 52, no. 4, pp. 1289–1306, Apr. 2006.

[18] C. S. Oxvig, P. S. Pedersen, T. Arildsen, J. Østergaard, and T. Larsen, "Magni: A Python Package for Compressive Sampling and Reconstruction of Atomic Force Microscopy Images," *Journal of Open Research Software*, vol. 2, no. 1, p. e29, Oct. 2014.